WILEY VCH

RESEARCH ARTICLE

Divergent Responses of Carbon Nitride Dot-Based Amorphous Species and Small Molecule Hybrids to Trace Level Analytes

Michael J. Holzmann[a], Eric R. Westphal[a], Kenneth M. Plackowski[a], Melissa L. Meyerson[a], John K. Grey[a], Koushik Ghosh[a]*

[a] MJ Holzmann, ER Westphal, KM Plackowski, JK Grey, K Ghosh
Sandia National Laboratory
1515 Eubank Dr. SE, Albuquerque, NM 87185
E-mail: kghosh@sandia.gov

Supporting information for this article is given via a link at the end of the document.

Abstract: Bottom-up synthesis of carbon nitride dots (CNDs) offers a versatile platform for the creation of diverse nanomaterials with tunable properties. Here, we report a facile hydrothermal approach using citric acid and urea as precursors to synthesize CNDs with varying degrees of condensation and crystallinity. By carefully controlling reaction conditions and post-synthetic treatments, we obtained two distinct fractions: a polycrystalline fraction composed of small-molecule hybrids and an amorphous fraction containing CNDs. We then sought to understand how the dominant species in these fractions impact sensing abilities using trace-level explosive exemplars. The results have important implications for sensing and related applications where understanding the complex interplay between synthetic conditions and post-synthetic processing play vital roles in determining the final properties of CND materials.

Introduction

Carbon nitride dots (CNDs)—a variant of carbon dots—have emerged as a promising class of nanomaterials with a wide range of applications, including sensing, optoelectronics, photocatalysis, and drug delivery.[1-4] Their popularity stems from the ease of synthesis, non-toxicity, and the abundance of suitable precursors, making them attractive for scalable production.[5-6] Unlike top-down synthesis methods, which often produce heterogeneous and polydisperse products, bottom-up approaches using small organic precursors under meticulously controlled conditions yields more homogeneous CNDs with smaller sizes and tunable surface functional groups. However, the bottom-up synthesis process is complex, involving multiple simultaneous condensation reactions that are challenging to monitor and define.[7-9]

One of the signature properties of CNDs is their excitation-dependent photoluminescence (PL). The origins of these PL transitions are multifaceted, with significant contributions from localized states of multiple orbital parentage, surface/edge states, and the formation of J- or H-aggregates of polyaromatic hydrocarbons.[10-12] Additionally, crosslinked enhanced emission (CEE)[13] and the presence of molecular fluorophores[14] or their aggregates play crucial roles. For example, recent studies have CNDs may be contaminated with organic molecular chromophores, particularly in samples subjected to insufficient carbonization.[15-18] This unintended contamination affects the spectroscopic properties, complicating the interpretation of CNDs' luminescence and targeted uses.[19]

In this work, we aim to address the critical challenge of understanding and optimizing the multi-variable space of bottom-up carbon dot synthesis for fluorescence-based sensing. By maintaining a sufficiently high heating duration (24 hours) at 160 °C, we ensure substantial carbonization[20-21] although substantial amounts of non-CND products may persist. We adapt a simple purification process that allows us to track all reaction products and yet provide a method to distinguish the small-molecular precursors from fused aromatic components and additionally, understand their interactions. We then investigate how specific reaction conditions influence the sensing abilities of CAU fractions when exposed to trace-level concentrations of exemplar explosive analytes, such as trinitrotoluene (TNT) and triacetone triperoxide (TATP), which leverages results from our previous work revealing analyte-and state-specific fluorescence quenching and enhancement patterns.[22] Our findings highlight the significance of multiple interacting emitting species and the need to address lingering questions regarding the influence of different species and their coupling, which can lead to apparent crosstalk in observed photoluminescence (PL) signals.

We selected citric acid (CA) and urea (U) as the condensing partners for the hydrothermal reaction. By maintaining the reaction time at 24 hours and a temperature of 160 °C, significant carbonization is realized while potential formation of multiple small-molecule species is also possible. Following purification by filtration, precipitation, and high-speed centrifugation in

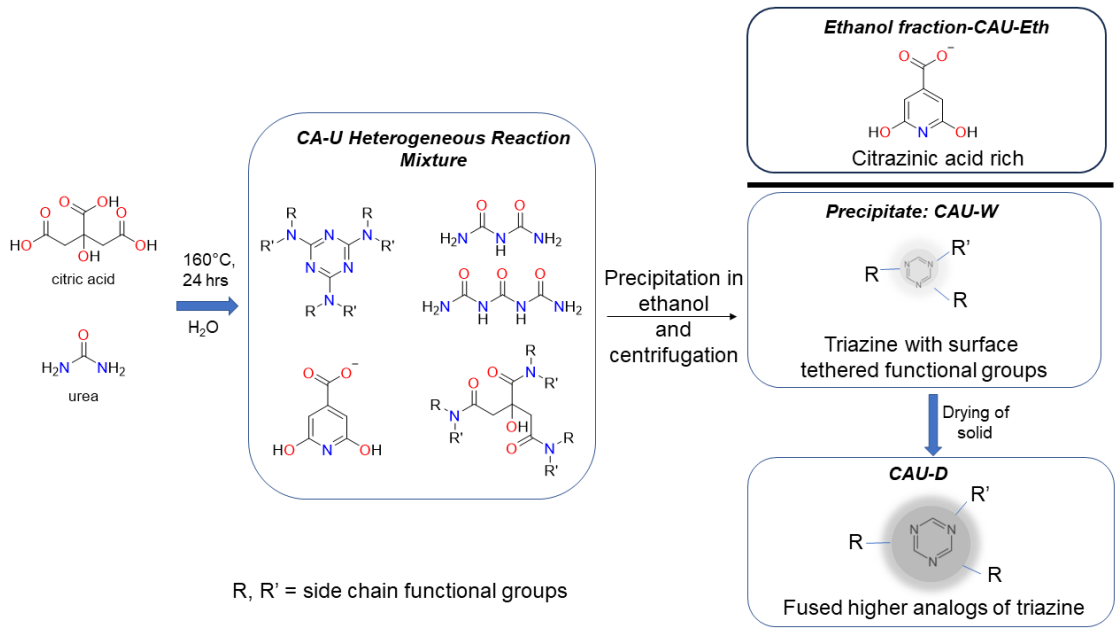

Scheme 1. (A) Hydrothermal treatment of citric acid (CA) and Urea (U) leads to a heterogenous reaction mixture, with precipitation and drying leading to a diverse carbon dot subset.

ethanol,[23] we obtained two major components: an ethanol fraction (CAU-Eth) and a wet fraction (CAU-W). The CAU-W fraction, saturated with both bulk and trapped water (Figure S15), underwent a series of dehydration-driven transformations during drying, followed by the evolution of ammonia, resulting in a more carbonized and dry species, referred to as CAU-D. The evolution of CAU-D with drying can be monitored spectroscopically to reveal the differences and similarities with the ethanol fraction. Differences in molecular composition produce changes in excitation-emission landscapes that offer views into analyte interactions. Specifically, we found that the CAU-Eth exhibited different responses to explosive analytes TNT and TATP compared to their highly carbonized CAU-D counterparts indicating the possibility of harnessing molecular promiscuity in the reaction mixture.[24-26]

Results and Discussion

As shown in Scheme 1, significant heterogeneity is expected from the hydrothermal reaction between citric acid (CA) and Urea (U), producing an array of carbon rich precursors ranging from polyamides to triazines to small molecular fluorophores. In particular, prior work has demonstrated the prevalence of citrazinic acid (CzA) as a common byproduct using this hydrothermal approach which can obscure development of carbon nitride structures.[27] Liquid state NMR characterization on a reaction mixture of CA and U after hydrothermal reaction prepared with D_2O revealed ^{13}C NMR shifts occurring at ~95, 154, 164, and 175 ppm (Figure S1) matching the resonances of citrazinic acid carboxylate (CzA-COO^-) [28]and C atoms (N2@CN or terminal CN2(NH_x)) in triazine units.[20] The typical signals corresponding to C atoms (CN3) in heptazine units at around 156 ppm are absent. Hence, NMR validates both triazine-based structure and citrazinic acid based small units in the reaction mixture. Additionally, the three distinct resonances around 180 ppm and shifts around 160 ppm likely is amides/esters/carbonamides possibly existing as a small molecule or as a surface tethered group of carbon nitride group. While the liquid-state NMR can be a good tool for affirming the heterogeneity of the reaction mixtures, it can be misleading due to the differences in relaxation times between the faster tumbling small-molecules and slower tumbling of larger solubilized carbonized species. Specifically, the latter effect leads to faster relaxation of transverse magnetization (short T_2) due to enhanced spin-spin interactions.[29] Additionally, CAU systems spontaneously aggregate and self-assemble in solution making liquid state NMR studies of both CAU-Eth and CAU-D unsuccessful due to the significantly longer relaxation and acquisition times necessary to capture all species.[30]

As shown in Figure 1A, infrared spectroscopy (IR) of both CAU-Eth and CAU-D show the broad bands centered at 3230 cm^{-1} and 2990 cm^{-1} are assigned to the stretching vibrations of N-H and O-H bonds, respectively, contributing to the hydrophilic nature of the CAU-D surface. The uncanny similarity between the citrazinic acid and CAU-Eth further corroborate our observation in NMR. Unfortunately, additional efforts to distinguish CAU-Eth and CAU-D by infrared spectroscopy were inconclusive because of the overlapping C=O (1650 cm^{-1}), C-N (1310 cm^{-1}), and C-O (1220 cm^{-1}) stretching signals with a marked difference in peak broadness in CAU-D vs. CAU-Eth. Raman Spectra were inconclusive as overwhelming photoluminescence (PL) background signals precluded the effective resolution of the CND framework (data not shown).[31]

In X-ray photoelectron spectroscopy (XPS) (Figure S13-S16), three spots on CAU-D were all consistent with a composition of 10 at% N, 29 at% O, and 61 at% C with adventitious C. The N 1s spectrum showed a main peak at 400.1 eV and a shoulder at 401.7 eV. The O 1s spectrum showed a main peak at 531.8 eV with a shoulder at 533.2 eV. The C 1s spectrum showed two clearly separated peaks, but likely contains additional

contributions. The lower binding energy peak is centered at 284.9, likely comprised of sp^2 C, sp^3 C, and C-O/C-N species. The higher binding energy peak is centered at 288.7 eV and is likely comprised of C=O and O-C=O species.

In contrast, three spots on CAU-Eth are less consistent with each other, which, along with the visually distinct colored regions present, suggests multiple materials are present. Some spots contain a single N 1s peak centered at 401 eV, others have a broader N 1s peak which include features at both higher and lower binding energy. Similarly, the O 1 spectrum, which likely contains multiple species, is centered closer to 533.1 eV for some spots and at a lower binding energy of 531.7 eV for others. Similar to the CAU-D, the C 1s spectrum for the CAU-Eth contains two distinct, but broad peaks (285.7 eV and 289.2 eV), which are likely comprised of multiple different components. The elemental composition for the CAU-Eth sample was 10 at% N, 33 at% O, and 57 at% C.

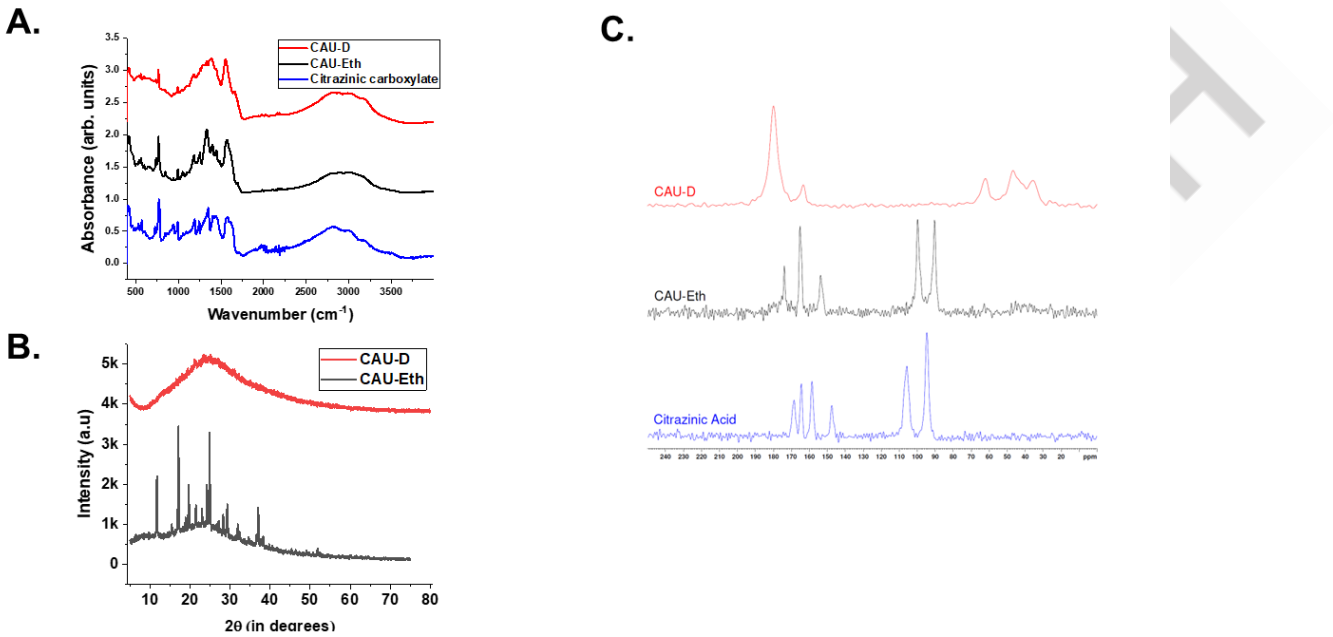

Figure 1. Structural Characterization: (A) IR absorption spectra of CAU-D, CAU-Eth, and reference citrazinic acid (B) Comparison of XRD of CAU-Eth and CAU-D species. (C) Solid-state NMR of the hydrothermal CAU-D and CAU-Eth, and citrazinic acid carboxylate (CzA-COO^-).

As shown in Figure 1B, CAU-D presents the least complex XRD pattern. The weak, diffuse peak is indicative of an amorphous structure, with a single discernible peak at 25.5° corresponding to a d-spacing of 0.35 nm. This value is slightly higher than the 0.34 nm spacing observed in planar carbon nitride, which typically exhibits a peak at 27° in XRD patterns.[32] The larger spacing in CAU-D can be attributed to its smaller particle size compared the more extended, planar structure of graphitic carbon nitride. CAU-Eth displays the most intricate XRD pattern with sharp, well-defined peaks indicative of crystalline structures. The numerous peaks, exceeding 25° with a signal-to-noise ratio greater than 3, suggest a polycrystalline sample. The intense peak at 11.1° (d-spacing of 0.8 nm), 17.5° (d-spacing of 0.51 nm), and 26.5° (d-spacing of 0.34 nm), reveal a systematic pattern in the spacings, likely resulting from a linker between the lattices. The multitude of smaller and sharper peaks with higher signal to noise ratio also hints at subtle structural variations characteristic of extreme heterogeneity in the CAU-Eth fraction. Overall, these results are consistent with citrazinic acid-rich species present in the ethanol fraction and fused triazine containing CND species mainly comprising the CAU-D solid fraction.

Optical microscopy (Figure S17-S21) provides a clear distinction between the amorphous morphological structure of CAU-D and the crystalline CAU-Eth structure. The amorphous CAU-D exhibits isotropic optical properties, which are characteristic of materials with random atomic arrangements and lack of long-range order, as seen in amorphous solids like glass. In contrast, the crystalline CAU-Eth structure demonstrates anisotropic optical properties due to its periodic atomic arrangement, which can interact with light differently depending on orientation. Under polarized light, CAU-Eth shows distinct birefringence with characteristic interference colors, confirming its crystalline nature, while CAU-D remains optically isotropic and appears dark under identical conditions, validating its amorphous character. Together, these techniques demonstrate how atomic-scale order (XRD) directly governs macroscopic optical behavior (microscopy), with CAU-D's disordered structure preventing directional light effects and CAU-Eth's crystalline lattice enabling orientation-dependent interactions.

The most conclusive evidence can be drawn from solid-state NMR analysis which provides atomic-level structural insights into the CAU-D and CAU-Eth fractions, corroborating and expanding upon the crystallographic (XRD) and vibrational (FT-IR) data (Figure 1C). Distinct molecular architectures emerge between the two fractions, reflecting differences in condensation, hydrogen content, and functional group composition.

In the CAU-D spectrum, the characteristic resonance at 165 ppm[33] is unequivocally assigned to sp^2-hybridized carbon atoms within triazine rings (C=N bonding environments), consistent with established chemical shifts for carbon nitride frameworks containing triazine motifs. This signature confirms the presence of fused aromatic nitrogen-rich heterocycles, a hallmark of extended carbon nitride networks. In contrast, the CAU-Eth fraction exhibits spectral features analogous to citrazinic acid, indicative of a less condensed molecular structure with higher hydrogen content and potential oxygen-containing functional groups.

Notably, the substantial disparity in ^{13}C T_1 relaxation times—60 s for CAU-D versus 5 s for CAU-Eth and citrazinic acid—underscores fundamental differences in molecular mobility and local environments.[34] The extended T_1 relaxation time observed in CAU-D is consistent with reduced molecular motion, a consequence of rigid, fused aromatic systems with extended π-conjugation. This rigidity, coupled with lower proton density due to dehydrogenation during condensation, limits dipolar relaxation efficiency. These observations collectively support the conclusion that CAU-D comprises hydrogen-deficient carbon nitride frameworks with long-range aromatic ordering, whereas CAU-Eth retains monomeric or oligomeric species with greater conformational flexibility.

The contributions of these functionalities on optical properties are now investigated using UV-Vis and fluorescence spectroscopy (Figure 2). UV-Vis spectra of CAU-W and CAU-Eth reveal distinct electronic properties and aggregation behaviors (Figure 2A). Both exhibit absorption bands in the 300-400 nm region, characteristic of π-π* transitions in conjugated systems. However, subtle differences emerge: CAU-W and CAU-D spectra resemble those of carbonaceous materials, while CAU-Eth shows a red-shifted, broadened peak with a shoulder, indicative of a heterogeneous mixture (Figure 2B). Both CAU-W and CAU-Eth exhibit low-energy aggregated states. Serial dilution experiments (Figure S22) further differentiate their aggregation mechanisms: CAU-Eth displays classical intermolecular aggregation, with dilution reducing the intensity of the low-energy band relative to the high-energy band. In contrast, CAU-W displays negligible dilution effects, suggesting that its low-energy states may be linked to the high-energy carbonized core. This hypothesis is supported by the blue-shift of the low-energy band upon drying CAU-W, indicating a reduction in low-energy state populations.

As noted by Liang et al.[15] , carbon nanoparticles typically exhibit stable, broad-range optical absorption spectra (350-800 nm or beyond) that are relatively unaffected by modifications such as nitrogen doping or surface functionalization. These spectral features are characteristic of various carbon-based nanomaterials, including multi-walled carbon nanotubes.[35-38] Therefore, the emergence of novel optical absorption features in carbonization-derived samples warrants careful investigation to exclude the possibility of contamination by molecular dyes or chromophores, especially those generated from mild thermal conditions.

Fluorescence spectroscopy further highlights the diverse structural features of CAU-Eth and CAU-W. All of the species have strong fluorescence signals with excitation dependent emission illustrated by two dimensional maps. While CAU-Eth exhibits an excitation-emission pattern reminiscent of citrazinic acid (CzA) aggregates, a direct comparison is challenging due to CzA's extreme sensitivity to environmental factors.[39-41] Given the expected heterogeneity of the ethanol fraction, it is likely that CzA is the dominant species contributing to the fluorescence, although the cross-talk between other small-molecule fractions cannot be entirely excluded. In contrast, CAU-W displays a more complex fluorescence pattern, with a low-energy emissive tail linked to the more intense core. Drying CAU-D samples resulted in increased emission intensity and a more localized fluorescence line shape and excitation-emission pattern. Preliminary time-correlated single photon counting experiments with a 394 nm LED excitation source confirm the larger relative yields in dried samples arising from longer fluorescence lifetimes, particularly at 450 and 500 nm emission wavelengths (Figure S40).

Our comprehensive structural and optical characterization reveals that CAU-Eth primarily consists of polycrystalline small-molecule species, while CAU-D is predominantly comprised of amorphous triazine units. The transition from CAU-W to CAU-D is particularly intriguing, suggesting a proximity-induced condensation process accompanied by a shift from sp^3 to sp^2 hybridization. The observed rapid burst of nucleation[8, 42] upon solvent evaporation strongly affirms the formation of carbon dots within the system. As the solvent is removed, the concentration of aromatic clusters and carbon-rich intermediates in the reaction medium increases sharply, quickly reaching and surpassing the critical supersaturation threshold necessary for nucleation. At this point, the Gibbs free energy barrier for nucleus formation is dramatically lowered, enabling the spontaneous and simultaneous emergence of numerous carbon dot nuclei.[43-44] This burst nucleation results in the formation of predominantly amorphous carbon dot structures, as the rapid aggregation and limited molecular mobility during solvent removal favor the assembly of disordered, rather than highly graphitic, carbon domains. This mechanistic sequence aligns with classical nucleation theory and recent insights into carbon dot synthesis, confirming that the interplay between supersaturation and Gibbs free energy is central to the efficient and reproducible generation of carbon dots in such systems. Additionally, this process resembles the formation of biomolecular condensates,

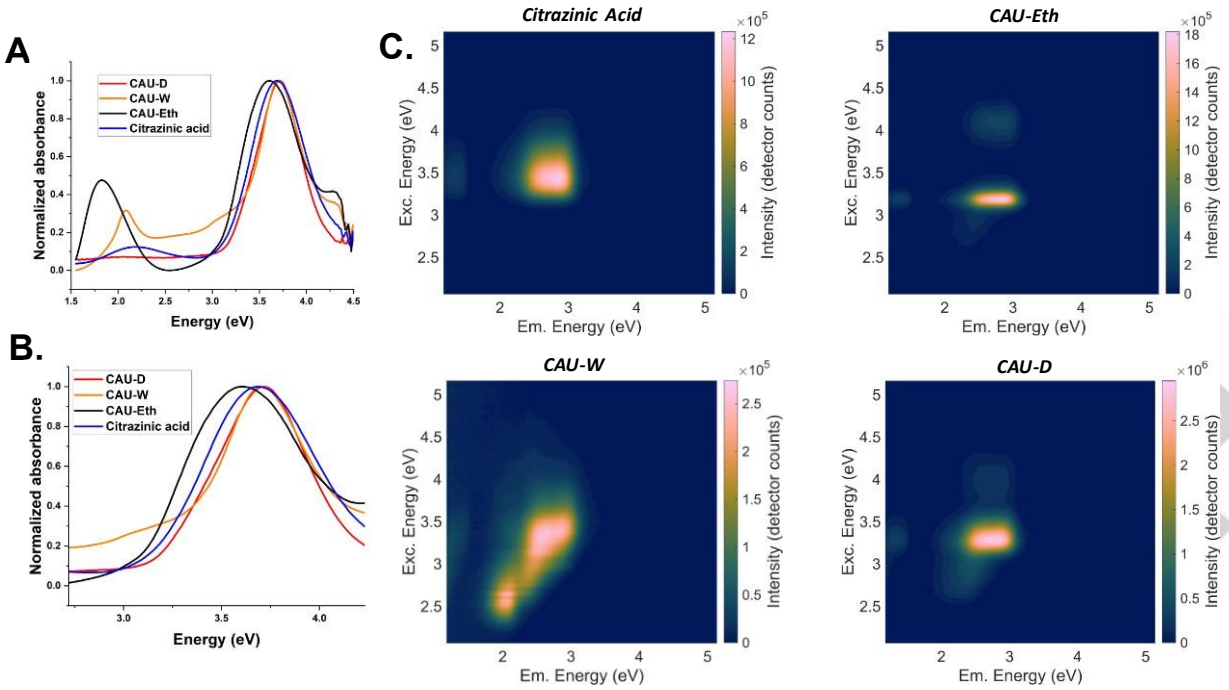

Figure 2. Optical characterization: (A) UV-Vis of CND fractions and citrazinic acid, (B) zoomed area of UV-Vis showing the distinct difference between CAU-Eth, CAU-D and CAU-W species, and (C) Excitation-Emission maps of the CAU-Eth, citrazinic acid, CAU-W and CAU-D

where biological systems utilize fusion, flow, and continuous material exchange in response to various stimuli.[45] Additionally, our findings align with the observations of Scott et al. regarding the impact of geometric distortions on the optical properties of polycyclic aromatic hydrocarbons.[46] These distortions, induced

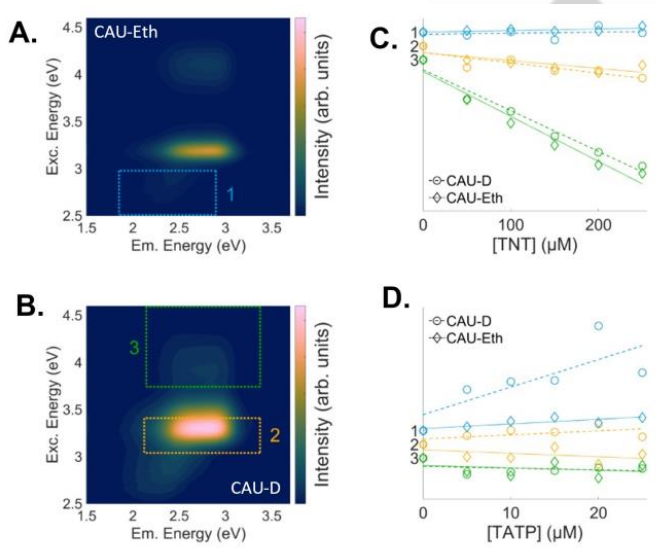

Figure 3. Differentiation and detection of explosive species by CAU-Eth and CAU-D: Excitation-emission maps and Stern−Volmer plots for each spectral region constructed using eq 1 for CAU-Eth and CAU-D species with TNT and TATP as trace analytes. These plots display integrated intensities from each region that are generated using the intensity ratios (I/I_0) and fitted using Stern-Volmer equation to obtain interaction constants.

by proximity effects, can lead to changes in emission spectra, similar to what we observe in our CND samples. While further investigation is necessary, these insights highlight the importance of considering the diverse emitting species present in CNDs and the role of structural factors in determining their optoelectronic properties.

Building upon insights relevant to the emissive properties of CAU fractions and our prior observations regarding trace-level analyte responses, we sought to address two primary questions: 1) Is it possible to exploit the distinct emissive species to detect and differentiate exemplary analytes? and 2) Can the drying-induced structural transformation support our previous hypothesis that strong oxidants (i.e., TATP) inhibit aggregation, thereby minimizing nonradiative decay pathways and enhancing fluorescence?

The methodology from our previous study was adapted,[22] which involved preparing two concentrations of CAU-Eth (0.25 and 0.06 mg/mL) and CAU-D (0.29 and 0.13 mg/mL) for assays with TNT and TATP analytes (Figures S24-S39). These analytes were selected based on their propensity to elicit strong quenching and enhancement responses, respectively, which suggest preferential interactions with specific CND species or functionalities. The carbon dot concentrations were maintained by adding 1.5 mL of the stock to five vials, followed by the addition of 100 µl aliquots of the explosive analyte. Each aliquot was then diluted to a total volume of 2 mL with methanol. Regions showing emission quenching/enhancement were selected for Stern-Volmer analysis using the equation,

$$\boldsymbol{I_0/I = -k_A \tau A/(1 + k_A \tau A)} \ldots\ldots (1)$$

where I and I_0 are fluorescence intensities with and without the analyte respectively, k_A is the bimolecular interaction rate constant, τ is the fluorescence lifetime in the absence of the analyte and A is the analyte concentration. Specifically, selected regions (4-4.5 eV (1), 3-3.5 eV (2), and 2.5-3 eV (3)) were integrated to create landscapes that highlight the excitation-dependent emission behavior depicting the overall change as a function of analyte addition (Figure 3). This approach captures

the nuanced variations in excitation energy influencing the emission response, providing a detailed understanding of the interaction dynamics between the CAU fractions and the analytes. For CAU-Eth and CAU-D, TNT elicited fluorescence quenching ($+k_A\tau A$) while TATP yielded distinct regions of quenching and enhancement ($-k_A\tau A$). As we identified previously,[22] diminished emission intensities for CNDs occurred on exposure to electron deficient aromatics (i.e. TNT); while peroxides (TATP) generated enhancements for states accessible at lower excitation energies. Further evidence suggests analyte induced fluorescence intensity modulation (AIFIM) can be tuned according to the physical state of the CAU species. For instance, interactions with TATP were more localized for CAU-Eth; with maximum enhancement and quenching occurring at region 1 and 2 respectively. Interestingly, the enhancement response of the primary emitting region 2 in CAU-D suggests post-synthetic modifications (i.e. drying) of CAU classes to be effective in selective analyte differentiation. This enhancement is even more pronounced in region 1 where we postulate the nature of the aggregating species is impacted by TATP. A quick comparison of the interaction constants (quenching/enhancement) in different regions (Table 1) show that while CAU-Eth and CAU-D have strong quenching effect with TNT across predominant emitting regions (area 2 and 3), the divergent responses become evident in response to TATP. These fractions exhibited distinct responses to explosive analytes, with both linear quenching and enhancement of state-specific indicative suggesting complex, internal competition and potentially preferential interactions with specific CND components. Similar to our previous observations, the absence of significant shifts in emission energies posits that reduced nonradiative rates are primarily responsible for the observed fluorescence enhancements. However, the nature of the enhancement pathway is more pronounced with CAU-D (5-fold greater than the CAU-24, from our previous observation[22]) which corroborate the hypothesis that the transformation from CAU-W (which is spectroscopically more similar to CAU-24) to CAU-D elicits a drastic change in the nature of the aggregating tail species in region 1, which is even more pronounced in the presence of TATP. We postulate that the interaction dynamics between our carbon nitride materials (CAU-Eth and CAU-D) and explosive analytes (TNT and TATP) arise from distinct photophysical pathways governed by molecular structure and material morphology. For TNT, its electron-deficient nitroaromatic system drives consistent fluorescence quenching across both CAU materials via photoinduced electron transfer (PET), where π-π stacking between TNT's aromatic rings and the sp^2-hybridized domains of CAU facilitates electron withdrawal, creating non-radiative decay channels. Quenching efficiency correlates with the material's graphitization degree, as increased structural order enhances electronic coupling. In contrast, TATP exhibits dual-mode behavior: its peroxide-rich structure induces region-specific enhancement through hydrogen bonding with surface hydroxyl/amine groups, suppressing non-radiative pathways in localized states, while simultaneous collisional quenching occurs in other regions due to steric interactions. CAU-Eth's crystalline, ordered framework confines TATP's enhancement primarily to region 1, with quenching dominant in region 2, reflecting well-defined interaction sites. These differential responses underscore how analyte electronic properties and material crystallinity synergistically dictate emissive state stabilization versus charge-transfer-mediated deactivation.

Table 1. Interaction constants ($k_A\tau$) for CAU-Eth and CAU-D with analytes TNT and TATP

$k_A\tau$, (M^{-1})	TNT			TATP		
	SR 1	SR 2	SR 3	SR 1	SR 2	SR 3
CAU-Eth	58.49	-285.53	-1633.07	1707.69	-1270.75	-874.85
CAU-D	39.14	-374.83	-1484.67	10062.43	1481.08	-631.46
CAU24[a]	82 ± 84	-207 ± 177	-239 ± 11	1780 ± 331	-389 ± 731	-88 ± 40
CAU6[a]	-31 ± 61	-206 ± 139	-109 ± 29	285 ± 333	-151 ± 702	12 ± 310

[a] Value taken from Reference 22, SR=Specific regions

Conclusion

Our investigation definitively resolves long-standing ambiguities in carbon nitride dot science by demonstrating how molecular architecture dictates functional divergence, even among spectrally similar species.[16, 47] Through strategic manipulation of hydrothermal synthesis and drying protocols, we engineered two structurally distinct carbon nitride dot fractions—small-molecule-rich CAU-Eth and carbonized CAU-D—that exhibit diametrically opposed responses to trace explosive analytes. Crucially, XRD patterns, optical micrographs, and solid-state NMR spectra unambiguously demonstrate that their nearly identical optical signatures mask fundamentally different lattice organizations and supramolecular packing arrangements, unmasking critical structural disparities that govern their sensing behavior.

This work establishes three transformative insights for the field. First, structural determinism over spectral similarity dismantles the persistent myth of carbon nitride dot homogeneity, revealing how minor synthetic variations yield distinct crystalline architectures with divergent charge-transfer pathways. Second, conventional fluorescence-based classification proves inadequate, as multimodal characterization emerges as an essential tool for decoding the structure-function relationships governing explosive sensing performance. Third, our methodology achieves targeted carbon nitride dot engineering through controlled carbonization rather than complex post-synthetic modifications(i.e., doping), establishing a blueprint for rational design of detection nanomaterials.

The CAU-Eth/CAU-D dichotomy demonstrates that precise control over molecular ordering and graphitization enables explosives detection with tunable selectivity thresholds, on-demand fluorescence quenching or reactivation mechanisms, and predictive performance optimization through precursor stoichiometry. By integrating insights from impurity-focused studies and supramolecular assembly research, we establish that design principles are essential to distinguish covalent carbon architectures from fluorescent byproducts, addressing fundamental controversies in nanomaterial characterization. As the field moves beyond serendipitous discovery, our methodology offers a pathway to engineer carbon nitride nanomaterials with predictable functionality for biosensing, photocatalysis, and optoelectronics.

Supporting Information

Supporting Information is available from the Wiley Online Library or from the author.

Acknowledgements

Authors thank Keith Fritzsching for consultation on the solid-state NMR.Any subjective views or opinions that might be expressed in this perspective do not necessarily represent the views of the U.S. Department of Energy (DOE) or the U.S. Government. This work was supported by the Laboratory Directed Research and Development program at Sandia National Laboratories, a multimission laboratory managed and operated by National Technology and Engineering Solutions of Sandia, LLC, a wholly owned subsidiary of Honeywell International, Inc., for the U.S. Department of Energy's National Nuclear Security Administration under Contract DE-NA0003525.

Keywords: Carbon nitride dots • Fluorescence • Sensing • Citrazinic acids • Triazine

References

[1] L. Dordevic, F. Arcudi, M. Cacioppo, M. Prato, *Nature Nanotechnology* **2022**, *17*, 112-130.
[2] H. Zhang, J. Zhang, W. Chen, M. Tao, X. Meng, Y. Zhang, G. Zuo, *Carbon Energy* **2024**, *6*, e463.
[3] L. Cheng, H. Zhang, X. Li, J. Fan, Q. Xiang, *Small* **2021**, *17*, 2005231.
[4] M. R. Patel, S. K. Kailasa, *ChemistrySelect* **2022**, *7*, e202201849.
[5] W. D. Li, Y. Liu, B. Y. Wang, H. Q. Song, Z. Y. Liu, S. Y. Lu, B. Yang, *Chinese Chemical Letters* **2019**, *30*, 2323-2327.
[6] J. Zhang, S. H. Yu, *Materials Today* **2016**, *19*, 382-393.
[7] D. Qu, Z. C. Sun, *Materials Chemistry Frontiers* **2020**, *4*, 400-420.
[8] F. Rigodanza, M. Burian, F. Arcudi, L. Dordevic, H. Amenitsch, M. Prato, *Nature Communications* **2021**, *12*, 2640.
[9] C. L. Xia, S. J. Zhu, T. L. Feng, M. X. Yang, B. Yang, *Advanced Science* **2019**, *6*, 1901316.
[10] V. Strauss, J. T. Margraf, C. Dolle, B. Butz, T. J. Nacken, J. Walter, W. Bauer, W. Peukert, E. Spiecker, T. Clark, D. M. Guldi, *Journal of the American Chemical Society* **2014**, *136*, 17308-17316.
[11] P. Cui, Y. Xue, *Molecular Physics* **2022**, *120*.
[12] N. J. Hestand, F. C. Spano, *Chem. Rev.* **2018**, *118*, 7069-7163.
[13] J. X. Sun, J. K. Yu, Z. J. Jiang, Z. H. Zhao, Y. Z. Xia, *Acs Omega* **2020**, *5*, 27514-27521.

[14] L. Shi, J. H. Yang, H. B. Zeng, Y. M. Chen, S. C. Yang, C. Wu, H. Zeng, O. Yoshihito, Q. Q. Zhang, **2016**, - *8*, - 14378.
[15] W. Liang, S. K. Sonkar, D. Saini, K. Sheriff, B. Singh, L. Yang, P. Wang, Y. P. Sun, *Small* **2023**, *19*, 2206680.
[16] J. B. Essner, J. A. Kist, L. Polo-Parada, G. A. Baker, *Chemistry of Materials* **2018**, *30*, 1878-1887.
[17] Y. Xiong, J. Schneider, E. V. Ushakova, A. L. Rogach, *Nano Today* **2018**, *23*, 124-139.
[18] M. Langer, M. Paloncyová, M. Medved, M. Otyepka, *Journal of Physical Chemistry Letters* **2020**, *11*, 8252-8258.
[19] M. Otten, M. Hildebrandt, R. Kühnemuth, M. Karg, *Langmuir* **2022**, *38*, 6148-6157.
[20] Z. Xing, K. Dong, N. Pavlopoulos, Y. Chen, L. Amirav, *Angewandte Chemie International Edition* **2021**, *60*, 19413-19418.
[21] C. Xia, S. Zhu, T. Feng, M. Yang, B. Yang, *Advanced Science* **2019**, *6*, 1901316.
[22] E. R. Westphal, K. M. Plackowski, M. J. Holzmann, A. M. Outka, D. Chen, K. Ghosh, J. K. Grey, *ACS Sensors* **2024**, *9*, 5763-5769.
[23] J. Zhan, R. Peng, S. Wei, J. Chen, X. Peng, B. Xiao, *ACS Omega* **2019**, *4*, 22574-22580.
[24] A. Di Pizio, M. Y. Niv, *Bioorganic & Medicinal Chemistry* **2015**, *23*, 4082-4091.
[25] Y. Y. Liu, J. O. Ebalunode, J. M. Briggs, *Journal of Molecular Graphics & Modelling* **2019**, *88*, 104-120.
[26] B. Mannervik, A. Runarsdottir, *Febs Letters* **2010**, *584*, 2565-2571.
[27] W. Kasprzyk, T. Swiergosz, S. Bednarz, K. Walas, N. V. Bashmakova, D. Bogdal, *Nanoscale* **2018**, *10*, 13889-13894.
[28] F. Yang, G. E. LeCroy, P. Wang, W. X. Liang, J. J. Chen, K. A. S. Fernando, C. E. Bunker, H. J. Qian, Y. P. Sun, *Journal of Physical Chemistry C* **2016**, *120*, 25604-25611.
[29] M. P. Foster, C. A. McElroy, C. D. Amero, *Biochemistry* **2007**, *46*, 331-340.
[30] T. G. Habteyes, E. R. Westphal, K. M. Plackowski, P. G. Kotula, M. L. Meyerson, S. L. White, W. C. Corbin, K. Ghosh, J. K. Grey, *Nano Letters* **2023**, *23*, 9474-9481.
[31] K. J. Mintz, M. Bartoli, M. Rovere, Y. Q. Zhou, S. D. Hettiarachchi, S. Paudyal, J. Y. Chen, J. B. Domena, P. Y. Liyanage, R. Sampson, D. Khadka, R. R. Pandey, S. X. Huang, C. C. Chusuei, A. Tagliaferro, R. M. Leblanc, *Carbon* **2021**, *173*, 433-447.
[32] Y. Zheng, Z. S. Zhang, C. H. Li, *Journal of Photochemistry and Photobiology a-Chemistry* **2017**, *332*, 32-44.
[33] B. Jürgens, E. Irran, J. Senker, P. Kroll, H. Müller, W. Schnick, *Journal of the American Chemical Society* **2003**, *125*, 10288-10300.
[34] Y. Hu, Y. Shim, J. Oh, S. Park, S. Park, Y. Ishii, *Chemistry of Materials* **2017**, *29*, 5080-5089.
[35] F. Bruno, A. Sciortino, G. Buscarino, M. Cannas, F. M. Gelardi, F. Messina, S. Agnello, *Applied Sciences-Basel* **2021**, *11*.
[36] C. C. B. M. S. Jeong, O. H. Cha, H. Jeong, J. H. Han, Y. C. Choi, K. H. An, K. H. Oh, K. K. Kim, Y. H. Lee, , **2008**, *3*, 101-108.
[37] R. K. S. K. D. Patel, H-W.Kim, , **2019**, *6*, 434-469.
[38] F. J. Chao-Mujica, L. Garcia-Hernández, S. Camacho-López, M. Camacho-López, M. A. Camacho-López, D. R. Contreras, A. Pérez-Rodríguez, J. P. Peña-Caravaca, A. Páez-Rodríguez, J. G. Darias-Gonzalez, L. Hernandez-Tabares, O. Arias de Fuentes, E. Prokhorov, N. Torres-Figueredo, E. Reguera, L. F. Desdin-García, *Journal of Applied Physics* **2021**, *129*, 163301.
[39] S. Mura, L. Stagi, L. Malfatti, C. M. Carbonaro, R. Ludmerczki, P. Innocenzi, *Journal of Physical Chemistry A* **2020**, *124*, 197-203.
[40] H. Schneider, V. Strauss, S. Vogl, M. Antonietti, S. Filonenko, *Chemphyschem* **2023**, *24*, e202300180.
[41] L. Stagi, S. Mura, L. Malfatti, C. M. Carbonaro, P. C. Ricci, S. Porcu, F. Secci, P. Innocenzi, *Acs Omega* **2020**, *5*, 10958-10964.
[42] M. Pykal, J. Nociarová, D. Řeha, J. Filo, M. Šebela, P. Zajíček, M. Paloncýová, C. Olla, F. Mocci, A. Cappai, C. M. Carbonaro, Z. Baďura, L. Zdražil, R. Zbořil, A. L. Rogach, M. Medveď, M. Otyepka, *Nanoscale* **2025**, *17*, 7780-7789.
[43] R. de Bruijn, J. J. Michels, P. van der Schoot, *The Journal of Chemical Physics* **2024**, *160*.
[44] N. T. K. Thanh, N. Maclean, S. Mahiddine, *Chem. Rev.* **2014**, *114*, 7610-7630.
[45] A. G. T. Pyo, Y. J. Zhang, N. S. Wingreen, *Proceedings of the National Academy of Sciences of the United States of America* **2023**, *120*, e2220014120.
[46] J. M. Scott, S. G. Dale, J. McBroom, T. Gould, Q. Li, *Journal of Physical Chemistry A* **2024**, *128*, 2003-2014.
[47] D. A. Sousa, M. N. Berberan-Santos, J. V. Prata, *Chemistry-a European Journal* **2024**, *30*, e202302955.

Entry for the Table of Contents

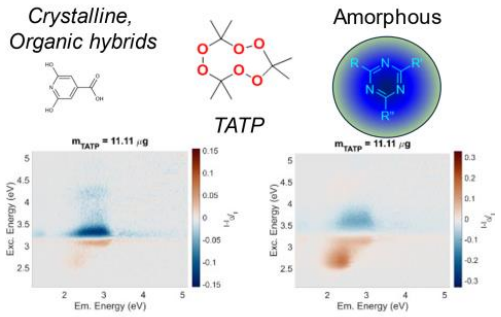

chem.202501495

Divergent Responses of Carbon Nitride Dot-Based Amorphous Species and Small Molecule Hybrids to Trace Level Analytes

TOC text:

This study presents a bottom-up synthesis method using hydrothermal reaction of citric acid and urea to produce carbon nitride dots with controllable properties. The approach yields two distinct fractions: polycrystalline small-molecule hybrids and amorphous carbon nitride dots. The research investigates how these different species affect explosive detection capabilities, providing insights for optimizing sensing applications through controlled synthesis conditions.